PEEC-Based Numerical Optimization of Compact Radial Position Sensors for Active Magnetic Bearings

Andreas MÜSING, Claudius ZINGERLI, Philipp IMOBERDORF, Johann W. KOLAR,
Power Electronic Systems Laboratory, ETH Zürich, Switzerland

Abstract

Eddy current sensors are widely used in active magnetic bearing systems to determine the position of the levitated rotor. This work is dealing with the numerical optimization of a radial eddy current position sensor to achieve a large output signal. A valid simulation model must be able to model the magnetic coupling between the sensor components as well as skin- and proximity effect. The Partial Element Equivalent Circuit (PEEC) method is best suited for these demands. In this paper, parameters of an existing sensor layout are investigated numerically, regarding the sensor output signal in dependency on parameters as excitation frequency and winding ratios. Furthermore, alternative layout geometries are discussed and compared to the classical sensor layout.

1 Introduction

1.1 Application Background

This work focuses on the analysis of the position detection system of a magnetic bearing for an ultra-high speed 1kW/500,000 rpm electrical machine (**Fig. 1**). Conventional ball bearings reach their mechanical limits for such extreme speeds: the increased friction losses lead to reduced system efficiency and finally to a short bearing lifetime. Therefore, the use of a magnetic bearing system is desired, which removes the mechanical friction problem. Further advantages of magnetic bearings are the lower accustic noise level and the capability of active damping of the rotor eigenmodes at critical rotation speeds. More details about applications, development and requirements of ultra-high speed machines can be found in [1-3]. Magnetic bearing systems need accurate and fast detection of the rotor position in all three spatial directions. An axial (*z*-position) measurement can be performed by standard eddy current sensors whereas the *x-y* measurement has higher demands on sampling frequency (> 100 kHz) and relative resolution (< 1 μm).
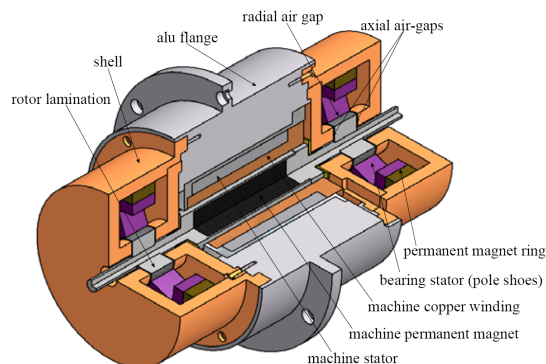

Fig. 1 Cut away view of the 1 kW / 500,000 rpm electrical machine.
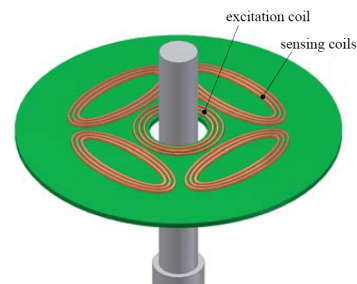

Fig. 2 3D CAD drawing of the sensor PCB capable of measuring the radial displacement of the rotor.

The limited speed and resolution of conventional eddy current sensors gives rise to use an alternative *x-y* position sensor approach, which was firstly introduced in [4].

1.2 Position Sensors

Conventional eddy current position sensors are placed around the rotor and generate a magnetic field, which is directed towards the rotating shaft. This allows the position detection by the measurement of the damping factor of a resonant circuit as the shaft changes its radial position. In [5] (**Fig. 2**), a novel type of radial sensor is presented where the sensor coils are integrated on a printed circuit board (PCB). A new aspect in that sensor is the separation into an excitation and sensing coils.

2.1.2 Sensor operating Mode and Theory

The examined position sensor layout consists of an excitation coil which is wound around the rotor and four sensing coils. The two opposing sensing coils are connected in anti-series, respectively. Hence, there is only a total induced voltage in the inductance series connection when the field strength on both sides is of different values.

The excitation coil is driven by a constant high frequency current in the MHz range and generates a concentric magnetic field. The rotor is electrically conductive (in our case titanium) and rejects the magnetic field by an eddy current around its axis (**Fig. 3a**). The induced eddy current can be considered as a current flowing in a single short circuit transformer winding concentric to the rotor axis. A rotor displacement in x- or y-direction results in an assymetric total magnetic field due to the superposition of the excitation field and the displaced field generated by the rotor eddy current (**Fig. 3b**). The schematic of the sensor circuit is depicted in **Fig. 4a** where the influence of the rotor on the sensing inductors is abstracted to a rotor position dependent mutual inductances $M_1(x)$ and $M_2(x)$.

For a practical sensor realization, two capacitors C_{pr} and C_{sec} are added, which form series resonant circuits on the primary (excitation) and secondary (sensing) side, respectively. The primary resonant circuit is used to generate the required alternating excitation current. As the secondary resonance is tuned to the excitation frequency, the obtained resonance magnification gives a measurable output voltage U_{out} at C_{sec}. The only relevant damping element in the secondary circuit is made up of the copper winding resistance on the PCB (including skin and proximity effect). The circuit simplification is depicted in **Fig. 4b**, where the primary side is simplified to an AC current source. This simplification is valid due to extremely small magnetic coupling k $\approx$ 0.001. The signal transmission is reduced to an effective mutual inductance difference $M_{eff} = M_1(x) - M_2(x)$, other components are simply merged. The output voltage magnitude is then calculated as

$$U_{out} = \frac{I_{sec}}{j\omega C_{sec}} = \frac{j\omega M_{eff}I_{pr}}{j\omega R_{sec}C_{sec} - \omega^2 LC_{sec} + 1} = \frac{M_{eff}I_{pr}}{R_{sec}C_{sec}} . \quad (1)$$

In this equation, the primary and secondary resonant frequency are given implicitly by C_{sec} and

$$f_{res} = \frac{1}{2\pi\sqrt{L_{sec}C_{sec}}} . \quad (2)$$

Therefore, an output energy optimization requires a maximum mutual inductance M_{eff} and a minimum secondary damping resistance R_{sec}. As discussed in the next sections, these are opposing requirements, and including skin- and proximity effect losses yields an optimum frequency for every sensor layout. I_{pr} is not considered in the optimization, because its magnitude is only restricted by the maximum PCB track current rating and therefore assumed as constant.

2.2   PEEC modeling

The Partial Element Equivalent Ciruit (PEEC) method is a numerical solution method of the Maxwell equations in integral form [6]. In comparison to FEM or FDM techniques, PEEC needs only the discretization of conducting areas or dielectrics [7] and it does not require any boundary conditions. Therefore, the number of solution variables is dramatically reduced in comparison to a corresponding FEM model, which makes PEEC best suited for the position sensor simulation. General PEEC cells are constituted by lumped partial inductances, capacitances and resistances, which are used to model the sensor
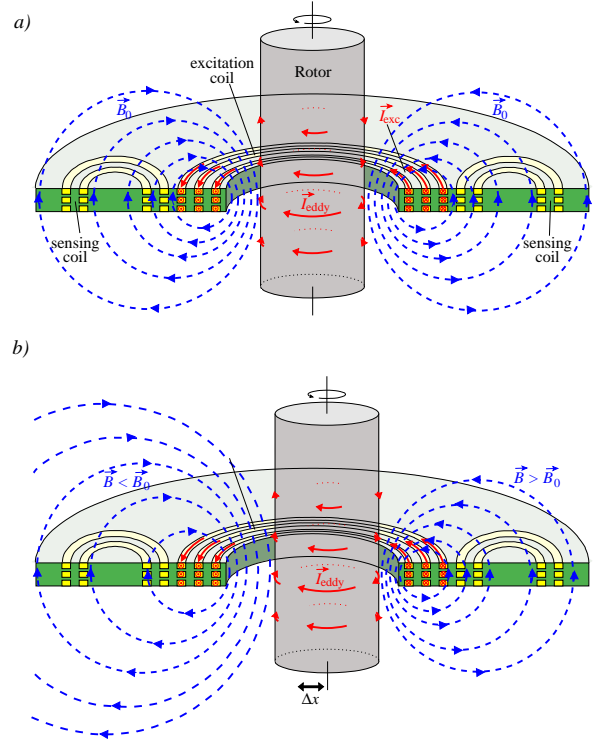

Fig. 3   Illustration of the position detection principle: The excitation coil generates an axial-symmetric magnetic field and induces an eddy current inside the rotor. For a centered rotor, the superimposed total field remains axial-symmetric (a), whereas a displacement Δx diminishes and amplifies the total field on the opposing sides, respectively (b). The magnetic field difference is then detected in the sensing coils.
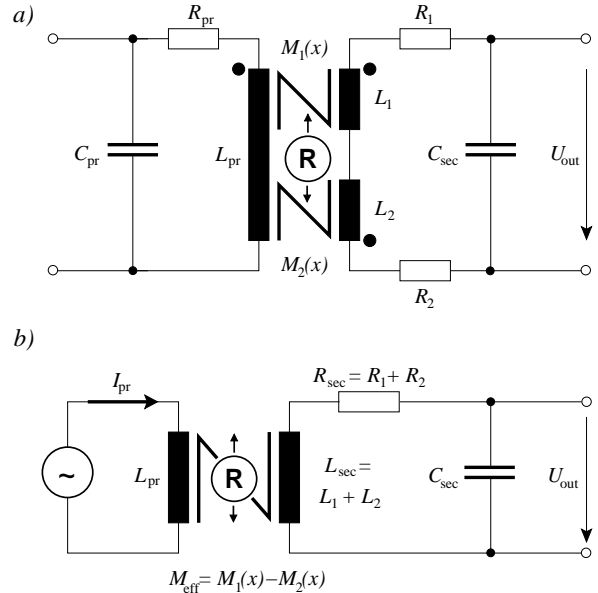

Fig. 4   a) Schematic of the PCB position sensor; the resistances are caused by the copper windings, whereas the capacitors are external components used to align the primary and secondary series resonant circuit frequency. b) Simplified equivalent circuit model: Merged components and, in particular, the mutual inductances are reduced to the difference due to a field assymetry caused by a rotor displacement.

PCB layout and the rotor. PEEC supports time domain as well as frequency domain (FD) simulations, here FD simulation is only used, which allows a very simple numeric analysis of the examined sensors.

2.2.2 Machine Rotor Model

The rotor is a 3 mm diameter titanium cylinder. Titanium is used because of its high strain capability, however the alloy conductivity $\sigma_{tit}= 4.7 \cdot 10^5$ $(\Omega m)^{-1}$ is, in comparison to copper ($\sigma_{cop}= 5.0 \cdot 10^7$ $(\Omega m)^{-1}$ at T = 70° C), extremely low. Hence, the resulting skin depth

$$\delta = \sqrt{\frac{2}{\omega \sigma \mu}} = \frac{1}{\sqrt{f \mu_0 \sigma \pi}} \qquad (3)$$

becomes accordingly large and a full volume PEEC model for the titanium rotor is required. The cylindrical rotor geometry is modeled by an octagonal shape, which is an adequate trade-off between accuracy and required PEEC cell number (**Fig. 5**). Here, the possibility to use nonorthogonal PEEC cells [8] is essentially, otherwise a large number of cubical cells would be needed to model the cylinder shape. The rotor geometry is built of a stack of octagonal PEEC cell layers (Fig. 5a). Since the induced eddy current density is declining with increasing *z*-distance to the sensor center, the PEEC cell stack does not require any further extension than shown in Figure 5. The discretization in radial direction is chosen according to the expected skin-effect, i.e. the the cell width becomes smaller towards the rotor surface (Fig. 5 b and c).

2.2.2 Excitation and Sensing Coil Models

The excitation and sensing coils of our test sensors are built on a 4-layer PCB with a centered drillhole for the machine rotor (**Fig. 6**). The use of a PCB is ideal for the position sensor in the face of production cost, alignment accuracy and reproducability. However, PCB manufacturers give some constraints on the layout geometries, in particular the minimum copper line width and the minimum distance between two seperated tracks are both 150 μm. These specifications are maintained for the following numeric and experimental sensor layout analysis.
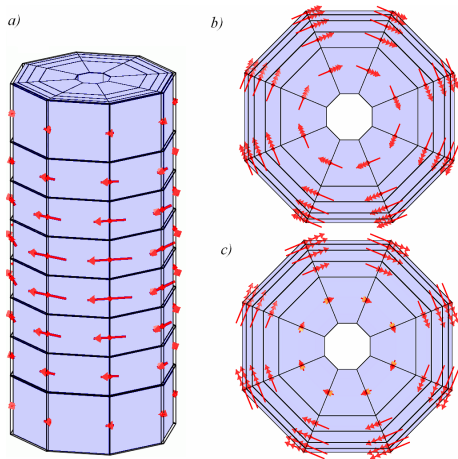

Fig. 5 Cell discretization of the PEEC model for the machine rotor. The red arrows display the simulated current densities: a) side view, b) top view at 50 kHz and b) 500 kHz excitation frequency.
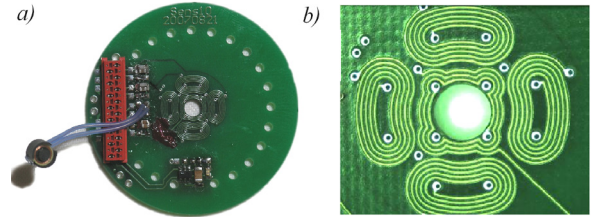

Fig. 6 a) Position sensor PCB with the connector, wiring, resonant capacitors and an attached conventional eddy current sensor for the *z*-position detection, b) magnified clipping of the radial sensor layout (referred to as layout A).
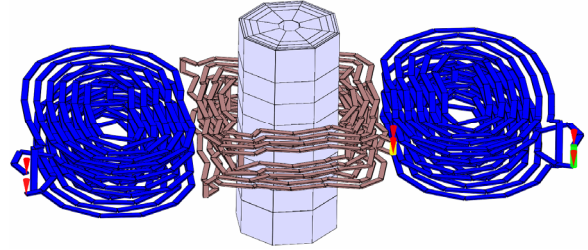

Fig. 7 PEEC simulation model of layout A.

For a practical sensor realization, the routing must consider the via placement and feed lines, whose forward and return paths should enclose a minimum area to minimize the stray inductance and the coupling of undesired signals.

The complete PEEC simulation model is shown in **Fig. 7**. Due to symmetry reasons, it is sufficient to consider only one pair of sensing coils, e.g. in *x*-direction. The PCB conductor paths are modeled as single discretization PEEC elements, hence proximity and skin effect are not modeled correctly for the coils. However, the exact current distribution within the 150 μm tracks has only negligible influence on the mutual inductance M_{eff}.

The evaluation of R_{sec} in (2) is strongly influenced by skin and proximity effect losses, see e.g. [10]. Therefore, a quantitative correct PEEC simulation would require a subdivision of all coil conductors into many cells. To avoid the resulting computational overhead for the evaluation of (2), the impedance measurement $R_{sec} = Re(Z_{sec})$ from **Fig. 8** is used to scale the corresponding DC damping resistances in the following section for different sensor layouts.
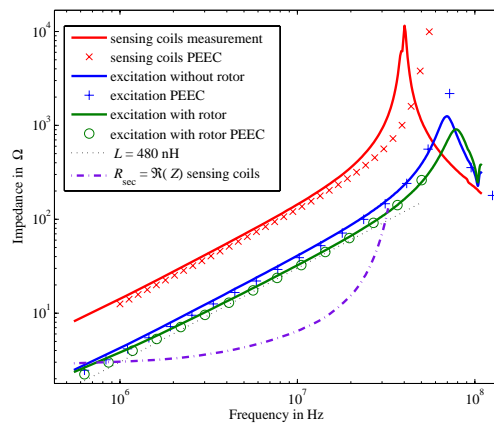

Fig. 8 Impedance measurements and simulation results obtained from a PEEC simulation of the layout from Fig. 6.

Furthermore, the inductances obtained from Fig. 8 show the validity of the simulation model: The simulated inductance values differ only within 3% compared to the measurements. The excitation coil impedance in Fig. 8 also shows the effect of the rotor which lowers the value $|Z|$ about 20%. For frequencies < 2 MHz this difference vanishes due to the increasing eddy current skin depth inside the rotor.

4 Simulation Results

4.1 General Sensor Properties

As a start, some general properties of the layout from Fig. 6 and Fig. 7 are presented. Distributed on 4 PCB layers, the sensor has 12 excitation and 2x20 sensing windings. **Fig. 9** shows the effective mutual inductance dependency on frequency and rotor displacement. The rise of M_{eff} with increasing frequency is caused by the rotor eddy current skin effect (Fig. 5): the more the eddy current is concentrated on the rotor surface, the better is the coupling. For high frequencies, a saturation of M_{eff} can be observed, since then the rotor eddy current can be assumed as surface current.

Some additional properties from Fig. 9 are noteworthy: M_{eff} shows an excellent linearity in rotor displacement. Additionally, the x- and y- signals are almost completely decoupled. The dashed curve in Fig. 9 shows M_{eff} for a rotor displacement of 100 μm in both, x and y direction which has only a minor effect in comparison to the original curve.

The dash-dotted line in Fig. 9 dennotes the effect of a non-ideal sensor layout, where the excitation windings are shifted away from the center position by 1 μm. The sensor signal is extremely sensitive to such a displacement, since the differential output signal relies on the compensation of the two sensing inductances.
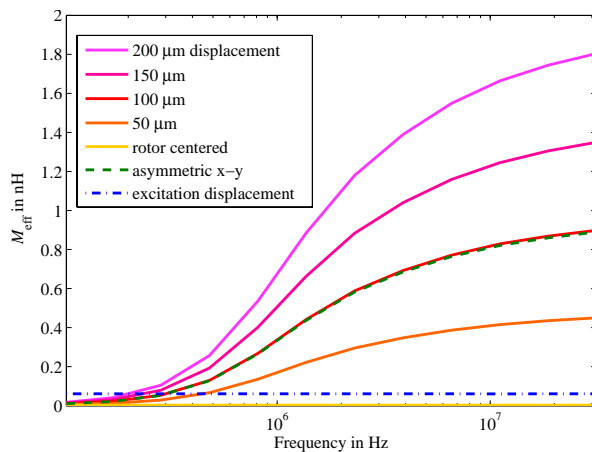
Fig. 9 Calculated effective mutual inductance M_{eff} in dependency on rotor displacement and frequency. The frequency influence is mainly caused by the eddy current skin effect inside the rotor.
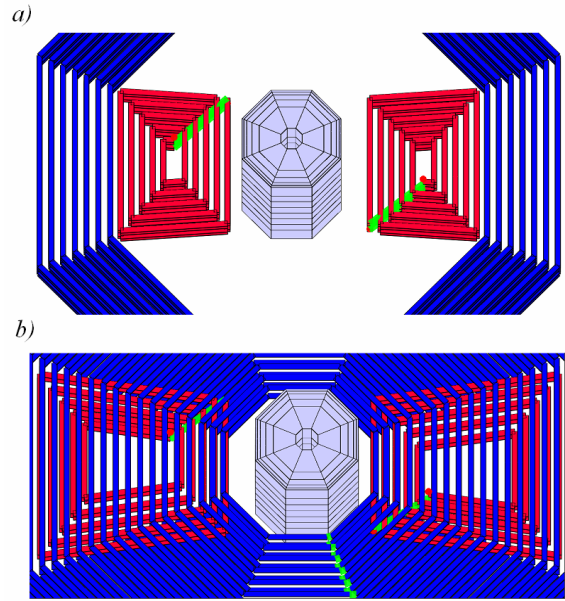
Fig. 10 Alternative sensor layouts: a) The sensing coils (red) are placed inside a larger excitation coil (layout B), b) the windings are overlapping and every coil occupies only 2 layers on the 4-layer PCB (layout C).

4.2 Sensor Layout Variation

The sensor layout has a wide number of optimization possibilities, e.g. an increased number of excitation windings amplifies the induced rotor eddy currents. But then, on the other hand, the distance between rotor and sensing windings has to be increased. A similar conclusion is valid for the number of sensing windings, where additionally the geometry and number of windings is related to the values of R_{sec} and L_{sec}.

In the following, the output voltages of different sensor layouts are compared, according to (1). For this comparison, the rotor displacement is fixed to 200 μm and a constant primary current amplitude of 100 mA is assumed.

Additionally to the conventional layout A as proposed in [5], two alternative topologies are shown in Fig. 10, which are referred to as layout B and C. In Fig. 10a, the placement of excitation windings and sensing coils is inverted, whereas layout type C has overlapping coil windings, distributed each on only 2 layers of the 4-layer PCB. The proposed new topologies have the advantage that an increase in the number of turns does not necessarily enlarge the distance between rotor and sensing windings.

The relative performance in output voltage of several different combinations of turns and layouts is summarized in **Table 1**, where the existing configuration from Fig. 6 is used as a reference. The results for type A show very limited optimization capabilities, whereas types B and C are clearly superior to the classical layout. The frequency dependent output voltages for some example layouts are summarized in **Fig. 11**.

Layout Type	No. of turns excitation	No. of turns sensing	Output signal gain to A1
A1	12	2x20	1
A2	16	2x20	1.05
A3	20	2x20	0.82
A4	16	2x24	0.94
B1	28	2x20	3.75
B2	32	2x16	2.75
B3	36	2x12	2.05
C1	40	2x8	2.04
C2	40	2x20	2.54

Table 1 Calculated performance (relative maximum output voltages) of different sensor layouts compared to the existing layout from Fig. 6.
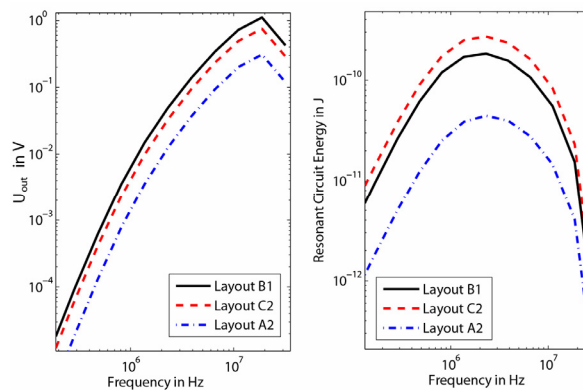

Fig. 7 Sensor output voltage and energy content of sensing resonance for different layouts from table 1.

The strong output signal increase with frequency in Fig. 11 has to be interpreted carefully, because part of the slope has its origin in the frequency dependent impedance of the secondary series capacitance, see equations (1) and (2). For an alternative comparison, the resonance energy in the sensing windings is plotted in the figure, too.

5   Conclusion and Outlook

This work discusses the theory and detailed the numerical properties of a novel position sensor for active magnetic bearings using the PEEC simulation method. The simulation results show that a maximization of the sensor output is possible with respect to excitation frequency and sensor layout on the PCB. Tuning the excitation frequency to an optimum turned out to be the most important procedure to improve the sensor.

Particularly for designing new position sensors for a different configuration as given in this paper, for example using different rotor material, diameter or maximum displacement, the proposed simulation method can help to find the optimum layout easily. The comparison between impedance measurements and PEEC simulations showed the validity of the model within some percent deviation.

However, the effective loss resistance in the sensing circuit was obtained by impedance measurements which is dominated by skin- and proximity losses at high frequencies. Therefore the accuracy of the presented results is probably limited by the measurement accuracy and the error introduced by scaling the corresponding value to different sensor geometries.

Future work that has to be done is to implement improved layout B1 that gives the best performance, and validate the results by further measurements.

6   Literature

[1] Zwyssig, C.; Dürr, M.; Hassler, D.; Kolar, J.W.: An Ultra-High-Speed, 500,000 rpm, 1 kW Electrical Drive System. Proc. 4th Power Conversion Conference Nagoya, Japan, 2007

[2] Imoberdorf, P.; Zwyssig, C.; Round, S.D.; Kolar, J.W.: Combined Radial-Axial Magnetic Bearing for a 1kW, 500,000 rpm Permanent Magnet Machine. Proc. 22nd Applied Power Elec. Conf., Anaheim, USA, Vol. 2, pp. 1434 – 1440, 2007.

[3] Kolar, J.W.; Zwyssig, C.; Round, S.D.: Beyond 1,000,000 rpm - Review on Mega-Speed Drive Systems. Proc. 9th Brazilian Power Electronics Conf., Blumenau, Brasil, 2007

[4] Bühler, P.: Device for Contact-Less Measurement of Distances in Multiple Directions. European Patent No. EP 1 422 492, June 10, 2004

[5] Larsonneur, R.; Bühler, P.: New Radial Sensor for Active Magnetic Bearings, 9th International Symposium on Magnetic Bearings, Lexington, USA, 2004.

[6] Ruehli, A.E.: Equivalent Circuit Models for Three-Dimensional Multiconductor Systems. IEEE Transactions on Microwave Theory and Techniques, Vol. 22 (3), pp. 216-221, 1974

[7] Ruehli, A.E.: Circuit models for threedimensional geometries including dielectrics. IEEE Trans. on Microwave Theory and Techniques, Vol 40 (7), pp. 1507-1516, 1992

[8] Ruehli, A.E.; Antonini, G; Esch, J.; Ekman, J; Mayo, A.: Nonorthogonal PEEC Formulation for Time- and Frequency-Domain EM and Circuit Modeling. IEEE Trans. on Elec. Comp., Vol 45 (2), pp. 167-176, 2003

[9] Grover, F.W.: Inductance Calculations, Dover Publications, New York 1973

[10] Niknejad, A.M.; Meyer, R.G: Analysis of Eddy-Current Losses Over Conductive Substrates with Applications to Monolithic Inductors and Transformers, IEEE Trans. on Microwave Theory and Techniques, Vol 49 (1), pp. 166-176, 2001